Multi-Constellation Signal Design Aided Affine Frequency Division Multiplexing for 6G Communication Systems

Ke Jiang[†], Ping Yang[†], Tony Q. S. Quek[‡], Zilong Liu[§], and Saviour Zammit[*],
[†]*University of Electronic Science and Technology of China*, Chengdu, China
jiangke@std.uestc.edu.cn, yang.ping@uestc.edu.cn
[‡]*Singapore University of Technology and Design, Singapore*
tonyquek@sutd.edu.sg
[§]*University of Essex, Colchester, United Kingdom*
zilong.liu@essex.ac.uk
[*]*University of Malta, Msida, Malta*
saviour.zammit@um.edu.mt

***Abstract*—As one of the novel waveforms recently proposed for future 6G communications, affine frequency division multiplexing (AFDM) is capable of combating the effects of the high Doppler and achieving full diversity over high mobility wireless channels. In this paper, hybrid multi-constellations for AFDM systems are proposed. A hybrid multi-constellation is obtained by eliminating points with the largest energy and by geometric interpolation among the signal points of the traditional single constellation. Two types of hybrid multi-constellation schemes, namely multi-constellation aided AFDM-Type 1 (MC-AFDM-T1) and multi-constellation aided AFDM-Type 2 (MC-AFDM-T2), are designed to improve AFDM system reliability. Monte Carlo simulations demonstrate that the proposed MC-AFDM-T1 and MC-AFDM-T2 schemes are capable of achieving better symbol error rate (SER) compared to that of the original-AFDM (Ori-AFDM).**

***Index Terms*—Affine frequency division multiplexing (AFDM), signal constellation, symbol error rate (SER), minimum Euclidean distance (MED), doubly selective channels.**

I. Introduction

Future communication systems in the upcoming sixth generation (6G) era must support a diverse set of wireless applications and services, such as vehicle-to-everything (V2X) communications, unmanned aerial vehicles (UAV) networks, high-speed railway communications, and low-earth-orbit (LEO) satellite systems [1]. In these use cases, reliable communications over high mobility channels are desired. This is due to the fact that high Doppler may destroy the orthogonality among subcarriers of the widely-used orthogonal frequency division multiplexing (OFDM)-based systems.

Recently, a novel multi-chirp waveform, namely affine frequency division multiplexing (AFDM), was proposed [2]–[5] to combat the doubly selective fading channels, whilst to achieve the full diversity. Moreover, AFDM can be easily built upon OFDM framework, making it an excellent 6G waveform candidate which is compatible with the legacy fourth generation (4G) long term evolution (LTE) and fifth generation (5G) New Radio systems. Existing works on AFDM are mainly focused on channel estimation and equalization [3], [5], and its applications in integrated sensing and communication (ISAC) [6]–[8]. The latter is in comparison to OFDM assisted ISAC systems [9], [10] by leveraging judiciously designed OFDM signals. Among many others, as an example, index modulation (IM)-aided OFDM signal designs [11]–[15] have been one of the research hotspots in the past decade.

Besides, there are schemes which enable new signal designs for OFDM [19], [20] and provide better error performance over some IM-based schemes. Specifically, in [19], a novel set partition modulation (SPM) was proposed, where partitioned and ordered subsets in the set partitions were used to form codewords. This leads to OFDM-SPM in which various constellations were used to distinguish between subsets in a set partition. Later in [20], another novel concept, index and composition modulation (ICM), was proposed by the same authors, where the indices of active/deactive codeword elements and compositions of an integer were used to encode information. Compared to OFDM-IM, enhanced spectral efficiency (SE) and error performance were achieved by OFDM with ICM (OFDM-ICM).

To the best of our knowledge, there are very few works on signal designs for AFDM systems. This motivates us to consider the multi-constellation optimization for AFDM to achieve improved error performance. The main contributions of this paper are summarized as follows:

- We propose the concept of hybrid multi-constellation, in which one of the subset constellations is obtained by eliminating the points with the largest energy of a conventional constellation, and the other is obtained through the optimal geometric interpolations that maximize the

This work is supported by the National Key R&D Program of China under Grant 2023YFE0115100, the Sichuan Science and Technology Program under Grant 2023NSFSC0457, the Fundamental Research Funds for the Central Universities under Grant 2242022k60006, and Meituan Academy of Robotics Shenzhen under Grant 231565.

The corresponding author is *Ping Yang (yang.ping@uestc.edu.cn)*

Euclidean distance to the other two constellations;
- We introduce two types of AFDM variants based on the hybrid multi-constellation, i.e., hybrid multi-constellation aided AFDM-Type 1 (MC-AFDM-T1) and hybrid multi-constellation aided AFDM-Type 2 (MC-AFDM-T2), which can maintain the given SE using lower order modulations, whilst achieving improved error performance;
- We analyze the normalized minimum Euclidean distance (MED) of the proposed MC-AFDM-T1 and MC-AFDM-T2 through extensive numerical results. In addition, the symbol error rate (SER) performance of the proposed MC-AFDM-T1 and MC-AFDM-T2 are evaluated under doubly selective fading channels, demonstrating the superiority of the MC-aided schemes.

Notations: Boldface uppercase letters, boldface lowercase letters and italics letters denote matrices, column vectors, and scalars, respectively. $\mathbb{C}$ denotes the complex filed. $(\cdot)^H$ and $(\cdot)^T$ denote the complex transpose and transpose, respectively. $\mathcal{P}$ denotes a set and its cardinality is $|\mathcal{P}|$. $\|\cdot\|_{\mathrm{F}}$ denotes the Frobenius norm operator.

II. AFDM and MC Signal Designs

A. A brief overview of AFDM

AFDM is based on the discrete affine Fourier transform (DAFT) [2]–[4], and its modulator maps a vector $\mathbf{x}$ of M-ary amplitude and phase modulation (APM) symbols to the time-domain as follows,

$$s_n = \frac{1}{\sqrt{N}} \sum_{m=0}^{N-1} x_m e^{j2\pi(c_1 n^2 + \frac{mn}{N} + c_2 m^2)}, n = 0, ..., N-1, \tag{1}$$

and the matrix form of (1) is

$$\mathbf{s} = \mathbf{\Lambda}_{c_1}^H \mathbf{F} \mathbf{\Lambda}_{c_2}^H \mathbf{x}, \tag{2}$$

where

$$\mathbf{\Lambda}_c = \mathrm{diag}([1, ..., e^{-j2\pi c n^2}, ..., e^{-j2\pi c(N-1)^2}]),\ c \in \{c_1, c_2\}, \tag{3}$$

here, c_1 and c_2 are AFDM parameters, $\mathbf{x} \in \mathbb{C}^{N\times 1}$, and

$$\mathbf{F} = \left[\frac{1}{\sqrt{N}} e^{-\frac{2\pi mn}{N}}\right] \tag{4}$$

is the discrete Fourier transform (DFT) matrix.

Then, similar to the prefix of OFDM, a chirp-periodic prefix (CPP) is added, and is defined as

$$s_n^{\mathrm{CPP}} = s_{N+n} e^{-j2\pi c_1(N^2+2Nn)},\ n = -L, ..., -1. \tag{5}$$

After the parallel to serial conversion, and the transmission over the channels, the received signal samples are

$$r_n = \sum_{l=0}^{\infty} s_{n-l} g_n(l) + z_n,\ n = 0, ..., N-1, \tag{6}$$

where

$$g_n(l) = \sum_{i=1}^{P} h_i e^{-j2\pi f_i n} \delta(l - l_i), \tag{7}$$

is the channel impulse response of sample n with delay l, P is the number of multi-path components, $h_i \sim \mathcal{CN}(0, \frac{1}{P})$, f_i, and l_i are the channel coefficient, the Doppler shift and the integer delay of the i-th path, respectively. Define $\epsilon_i \triangleq N f_i = \alpha_i + \beta_i$ as the Doppler shift normalized with respect to the subcarrier spacing Δf [4], where $\alpha_i \in [-\alpha_{\max}, \alpha_{\max}]$ and $\beta_i \in (-0.5, 0.5]$ are the integer and fractional parts of ϵ_i, respectively. And it is assumed that the maximum channel delay $l_{\max} \triangleq \max(l) < N$, and that $L > l_{\max} - 1$.

After CPP removal, (6) can be written in the matrix form

$$\mathbf{r} = \mathbf{H}\mathbf{s} + \mathbf{z}, \tag{8}$$

where $\mathbf{r} = [r_0, r_2, ..., r_{N-1}]^T$, $\mathbf{s} = [s_0, s_2, ..., s_{N-1}]^T$, $\mathbf{z} = [z_0, z_2, ..., z_{N-1}]^T$ are received signal vector, the transmit signal vector and the received the noise vector, respectively. The matrix $\mathbf{H}$ in (8) is given by

$$\mathbf{H} = \sum_{i=1}^{P} h_i \mathbf{\Omega}_i \mathbf{\Xi}_{f_i} \mathbf{\Pi}^{l_i} \in \mathbb{C}^{N\times N}, \tag{9}$$

where $\mathbf{\Omega}_i = \mathrm{diag}([\omega_0, ..., \omega_n, ..., \omega_{N-1}]) \in \mathbb{C}^{N\times N}$ is a diagonal matrix and its elements are given as

$$\omega_n = \begin{cases} e^{-j2\pi c_1[N^2 - 2N(l_i - n)]}, n < l_i \\ 1, n \geq l_i \end{cases}, n = 0, ..., N-1, \tag{10}$$

$\mathbf{\Xi}_{f_i} = \mathrm{diag}([1, ..., e^{-j2\pi f_i n}, ..., e^{-j2\pi f_i (N-1)}]) \in \mathbb{C}^{N\times N}$ and $\mathbf{\Pi}$ is a permutation matrix given by

$$\mathbf{\Pi} = \begin{bmatrix} 0 & \cdots & 0 & 1 \\ 1 & \cdots & 0 & 0 \\ \vdots & \ddots & \vdots & \vdots \\ 0 & \cdots & 1 & 0 \end{bmatrix}. \tag{11}$$

After AFDM demodulation, the DAFT-domain signal is

$$\mathbf{y} = \mathbf{\Lambda}_{c_2} \mathbf{F} \mathbf{\Lambda}_{c_1} \mathbf{r} = \mathbf{H}_0 \mathbf{x} + \tilde{\mathbf{z}}, \tag{12}$$

where $\mathbf{H}_0 \triangleq \mathbf{\Lambda}_{c_2} \mathbf{F} \mathbf{\Lambda}_{c_1} \mathbf{H} \mathbf{\Lambda}_{c_1}^H \mathbf{F}^H \mathbf{\Lambda}_{c_2}^H$ and $\tilde{\mathbf{z}} = \mathbf{\Lambda}_{c_2} \mathbf{F} \mathbf{\Lambda}_{c_1} \mathbf{z}$ are the effective equivalent channel matrix and the equivalent noise vector, respectively. With $\mathbf{H}_0$, signal detection is performed to recover the AFDM transmit vectors according to the following maximum likelihood (ML) criterion,

$$\hat{\mathbf{x}} = \underset{\mathbf{x}\in\mathcal{X}}{\mathrm{argmin}} \|\mathbf{y} - \mathbf{H}_0 \mathbf{x}\|_{\mathrm{F}}^2, \tag{13}$$

and $\mathcal{X}$ is the set of all legitimate AFDM transmit vectors.

B. Multi-Constellation Signal Designs

In this part, we will present the principles of MC-AFDM-T1 and MC-AFDM-T2. In our design, the hybrid constellations are obtained through the optimal geometric interpolations and point eliminations. In the following subsections, the proposed MC-AFDM-T1 scheme employing M-ary APM modulation, which has the length of N, is denoted by MC-AFDM-T1-(N, M). Similarly, the MC-AFDM-T2 with N and M, and the Ori-AFDM with N and M are denoted by MC-AFDM-T2-(N, M) and Ori-AFDM-(N, M), respectively.

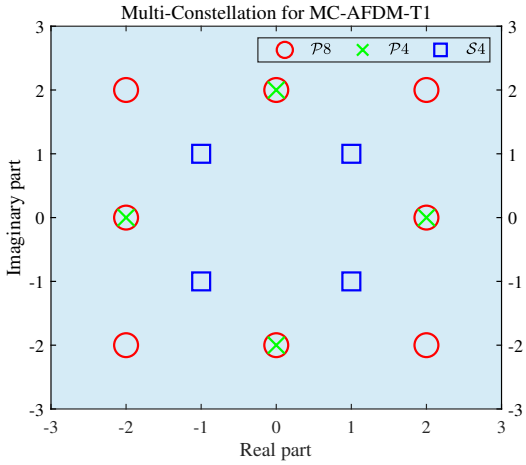

Fig. 1. The hybrid multi-constellation for MC-AFDM-T1 with $M = 8$, where the red circles, green crosses, blue squares represent the points of $\mathcal{P}8$, $\mathcal{P}4$ and $\mathcal{S}4$, respectively.

1) MC-AFDM-T1:

Firstly, we consider the example of MC-AFDM-T1-$(4, 8)$. Fig. 1 shows the multi-constellation for MC-AFDM-T1 with $M = 8$. Here the hybrid constellation is composed of three subconstellations, namely, $\mathcal{P}8$ (red circles), $\mathcal{P}4$ (green crosses) and $\mathcal{S}4$ (blue squares), respectively. $\mathcal{P}8$ is usually a conventional $M(=8)$-ary APM constellation and it is termed as the primary subconstellation. Then, based on $\mathcal{P}8$, the 2-nd subconstellation $\mathcal{P}4$ is obtained by eliminating the outermost $M/2 = 4$ points of $\mathcal{P}8$ with the largest symbol energy, i.e., $\{\pm 2 \pm j2\}$. Finally, the 3-rd subconstellation $\mathcal{S}4$ of $M/2 = 4$ points is obtained through the optimal geometric interpolations that maximize the Euclidean distances of both the sets of $\mathcal{P}8$ and $\mathcal{P}4$. Note here, for this multi-constellation composed of $\mathcal{P}8$, $\mathcal{P}4$ and $\mathcal{S}4$, its modulation order is equal to that of the primary constellation, i.e., 8, not the number of all symbol points, i.e., 16.

Furthermore, as shown in Fig. 1, the intra-MEDs of the three subconstellations are

$$d_{\text{MED}}(\mathcal{P}8) = d_{\text{MED}}(\mathcal{P}4) = d_{\text{MED}}(\mathcal{S}4) = d_0, \tag{14}$$

respectively, and the inter-MEDs between these constellations are

$$d_{\text{MED}}(\mathcal{P}8, \mathcal{S}4) = d_{\text{MED}}(\mathcal{P}4, \mathcal{S}4) = d_0/\sqrt{2}, \tag{15}$$

respectively[1]. That is to say, the MEDs of $\mathcal{P}8$, $\mathcal{P}4$ and $\mathcal{S}4$ are the same and equal to d_0. But the MEDs between $(\mathcal{P}8, \mathcal{S}4)$ and $(\mathcal{P}4, \mathcal{S}4)$ are $d_0/\sqrt{2}$, smaller than d_0. This suggests that the introduction of $S4$ reduces the MEDs of the hybrid constellation of $\mathcal{P}8$, $\mathcal{S}4$ and $\mathcal{P}4$, and eventually leads to degraded error performance. Thus, in order to preserve the MED of d_0, the number of elements of each vector $\mathbf{x}$ that take their values from $\mathcal{S}4$ has to be even. And only the case of two distinct AFDM vectors that differ by at least two elements can preserve the MED of d_0. With this constraint, all legitimate vector patterns for $\mathbf{x} \in \mathbb{C}^{4\times 1}$ of (2) can be represented by a set $\mathcal{L}_4 = \{\mathbf{x}_1, \mathbf{x}_2, ..., \mathbf{x}_8\}$ and the patterns in $\mathcal{L}_4$ are given by

$$\mathbf{x}_1 = [P_8, P_8, P_4, P_4]^T, \tag{16}$$

$$\begin{aligned} \mathbf{x}_2 &= [P_8, S_4, P_4, S_4]^T, \\ \mathbf{x}_3 &= [S_4, P_8, P_4, S_4]^T, \\ \mathbf{x}_4 &= [S_4, S_4, P_8, P_4]^T, \\ \mathbf{x}_5 &= [P_8, P_4, S_4, S_4]^T, \\ \mathbf{x}_6 &= [P_8, S_4, S_4, P_4]^T, \\ \mathbf{x}_7 &= [S_4, P_8, S_4, P_4]^T, \end{aligned} \tag{17}$$

and

$$\mathbf{x}_8 = [S_4, S_4, S_4, S_4]^T. \tag{18}$$

Specifically,

- for the pattern-$\mathbf{x}_1$ expressed in (16), no elements take values from $\mathcal{S}4$. In this pattern, six information bits are mapped to two $P8$ symbols, and four information bits are mapped to two $P4$ symbols. Therefore, pattern-$\mathbf{x}_1$ can convey a total of ten information bits;
- for the pattern-$\mathbf{x}_2 \sim \mathbf{x}_7$ expressed in (17), two out of the four elements take values from $\mathcal{S}4$. In each of these six patterns, three bits are mapped to one $P8$ symbol, two bits are mapped to one $P4$ symbol and four bits are mapped to two $S4$ symbols. Therefore, each of pattern-$\mathbf{x}_2 \sim \mathbf{x}_7$ can convey a total of nine bits;
- for the pattern-$\mathbf{x}_8$ expressed in (18), all the four elements take values from $\mathcal{S}4$. In this pattern, eight bits are mapped to four $S4$ symbols. Therefore, pattern-$\mathbf{x}_8$ can convey a total of eight bits.

Note that $\mathcal{P}8$ denotes a constellation set and P_8 denotes a symbols point in $\mathcal{P}8$. These two notations are also used for other signal constellations and symbol points.

For the patterns in $\mathcal{L}_4$, pattern-$\mathbf{x}_1$ can convey ten bits, each of pattern-$\mathbf{x}_2 \sim \mathbf{x}_7$ can convey nine bits, and pattern-$\mathbf{x}_8$ can convey eight bits. Thus, on average, one pattern in set $\mathcal{L}_4$ can convey $(10 + 9 \times 6 + 8)/8 = 9$ bits. Additionally, three more bits are required to choose one out of the eight patterns for bit-to-symbol mappings. And the SE of MC-AFDM-T1-$(4, 8)$ is calculated by $\eta_{\text{T1-}(4,\,8)} = (9 + 3)/4 = 3$ bits/s/Hz.

According to Fig. 1, the average symbol energy of $\mathcal{P}8$, $\mathcal{P}4$ and $\mathcal{S}4$ can be calculated as $E_{\mathcal{P}8} = 6$, $E_{\mathcal{P}4} = 4$ and $E_{\mathcal{S}4} = 2$, respectively. Thus the average (ave) energy of the vector patterns in set $\mathcal{L}_4$ is

$$\begin{aligned} E_{\text{ave}}^{\mathcal{L}_4} &= \frac{1}{|\mathcal{L}_4|}(E_{\mathbf{x}_1} + E_{\mathbf{x}_2} + ... + E_{\mathbf{x}_8}) \\ &= \frac{2E_{\mathcal{P}8} + 2E_{\mathcal{P}4}}{8} + \frac{4E_{\mathcal{S}4}}{8} \cdots\cdots (\text{for } \mathbf{x}_1, \mathbf{x}_8) \\ &+ \frac{6(E_{\mathcal{P}8} + E_{\mathcal{P}4} + 2E_{\mathcal{S}4})}{8} \cdots\cdots (\text{for } \mathbf{x}_2 \sim \mathbf{x}_7) \\ &= 14. \end{aligned} \tag{19}$$

Then, we have $E_1 = E_{\text{ave}}^{\mathcal{L}_4} = 14$ for MC-AFDM-T1-$(4, 8)$, and $E_2 = N \times E_{\mathcal{P}8} = 24$ for Ori-AFDM-$(4, 8)$, respectively. Furthermore, with $d_0 = 2$ in Fig. 2, the normalized MEDs of MC-AFDM-T1-$(4, 8)$ and Ori-AFDM-$(4, 8)$ are

$$d_1 = d_0/\sqrt{E_1} = 2/\sqrt{14} \approx 0.53, \tag{20}$$

[1]Here $d_0 = 2$ for the $\mathcal{P}8$, $\mathcal{P}4$ and $\mathcal{S}4$ shown in Fig. 1 and its value may vary when a different primary constellation is selected.

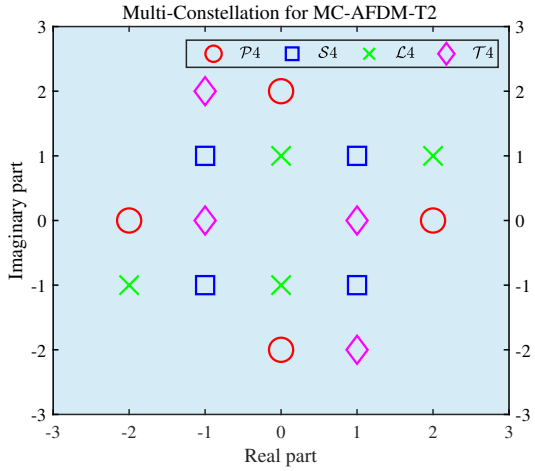

Fig. 2. The hybrid multi-constellation for MC-AFDM-T2 with $M = 4$, where the red circles, blue squares, green crosses and pink diamonds represent the points of $\mathcal{P}4$, $\mathcal{S}4$, $\mathcal{L}4$ and $\mathcal{T}4$, respectively.

and

$$d_2 = d_0/\sqrt{E_2} = 2/\sqrt{24} \approx 0.41, \tag{21}$$

respectively. Theoretically, (20) and (21) suggest that better error performance can be achieved by utilizing the MC-AFDM-T1-$(4, 8)$.

Similarly, we consider MC-AFDM-T1-$(6, 8)$ as another example. Under the delay-Doppler profile of $l_{\max} = 1$ and $\epsilon_{\max} = 1$, full diversity[2] can be achieved with $N = 6$. All legitimate vector patterns of MC-AFDM-T1-$(6, 8)$ can be represented by a set $\mathcal{L}_6 = \{\mathbf{x}_1, \mathbf{x}_2, ..., \mathbf{x}_{32}\}$ and the patterns in set $\mathcal{L}_6$ are given by

$$\mathbf{x}_1 = [P_8, P_8, P_8, P_4, P_4, P_4]^T, \tag{22}$$

$$\begin{aligned} \mathbf{x}_2 &= [S_4, P_8, P_8, P_4, P_4, S_4]^T, \\ \mathbf{x}_3 &= [S_4, P_8, S_4, P_8, P_4, P_4]^T, \\ &\cdots \\ \mathbf{x}_{16} &= [S_4, P_8, P_8, S_4, P_4, P_4]^T, \end{aligned} \tag{23}$$

$$\begin{aligned} \mathbf{x}_{17} &= [S_4, S_4, P_8, P_4, S_4, S_4]^T, \\ \mathbf{x}_{18} &= [S_4, S_4, P_8, S_4, S_4, P_4]^T, \\ &\cdots \\ \mathbf{x}_{31} &= [S_4, S_4, P_8, S_4, S_4, P_4]^T, \end{aligned} \tag{24}$$

and

$$\mathbf{x}_{32} = [S_4, S_4, S_4, S_4, S_4, S_4]^T. \tag{25}$$

Specifically,

- for the pattern-$\mathbf{x}_1$ expressed in (22), no elements take values from $\mathcal{S}4$. In this pattern, nine information bits are mapped to three $P8$ symbols and six information bits are mapped to three $P4$ symbols. Therefore, pattern-$\mathbf{x}_1$ can convey a total of fifteen bits;
- for the pattern-$\mathbf{x}_2 \sim \mathbf{x}_{16}$ expressed in (23), two out of the six elements take values from $\mathcal{S}4$. In each of these fifteen patterns, six bits are mapped to two $P8$ symbols, four bits are mapped to two $P4$ symbols and four bits are mapped to two $S4$ symbols. Therefore, each of pattern-$\mathbf{x}_2 \sim \mathbf{x}_{16}$ can convey a total of fourteen bits;
- for the pattern-$\mathbf{x}_{17} \sim \mathbf{x}_{31}$ expressed in (24), four out of the six elements take values from $\mathcal{S}4$. In each of these fifteen patterns, three bits are mapped to one $P8$ symbol, two bits are mapped to one $P4$ symbol and eight bits are mapped to four $S4$ symbols. Therefore, each of pattern-$\mathbf{x}_{17} \sim \mathbf{x}_{31}$ can convey a total of thirteen bits;
- for the pattern-$\mathbf{x}_{32}$ expressed in (25), all the six elements take values from the $\mathcal{S}4$. In this pattern, twelve bits are mapped to six $S4$ symbols. Therefore, pattern-$\mathbf{x}_{32}$ can convey a total of twelve bits.

Thus, on average, one vector pattern in set $\mathcal{L}_6$ can convey $\frac{15+14\times15+13\times15+12}{32} = 13.5$ bits. Additionally, $\log_2|\mathcal{L}_6| = \log_2 32 = 5$ more bits are required to choose a pattern out of the 32 patterns. And the SE of MC-AFDM-T1-$(6, 8)$ is $\eta_{\text{T1-(6,8)}} = \frac{13.5+5}{6} \approx 3.08$ bits/s/Hz.

In addition, the average energy of the patterns in $\mathcal{L}_6$ is

$$\begin{aligned} E_{\text{ave}}^{\mathcal{L}_6} &= \frac{1}{|\mathcal{L}_6|}(E_{\mathbf{x}_1} + E_{\mathbf{x}_2} + \cdots + E_{\mathbf{x}_{32}}) \\ &= \frac{3E_{\mathcal{P}8} + 3E_{\mathcal{P}4}}{32} + \frac{6E_{\mathcal{S}4}}{32} \cdots\cdots (\text{for } \mathbf{x}_1, \mathbf{x}_{32}) \\ &+ \frac{15(2E_{\mathcal{P}8} + 2E_{\mathcal{P}4} + 2E_{\mathcal{S}4})}{32} \cdots\cdots (\text{for } \mathbf{x}_2 \sim \mathbf{x}_{16}) \\ &+ \frac{15(E_{\mathcal{P}8} + E_{\mathcal{P}4} + 4E_{\mathcal{S}4})}{32} \cdots\cdots (\text{for } \mathbf{x}_{17} \sim \mathbf{x}_{31}) \\ &= 21, \end{aligned} \tag{26}$$

thus, we have $E_1 = E_{\text{ave}}^{\mathcal{L}_6} = 21$ for MC-AFDM-T1-$(6, 8)$ and $E_2 = N \times E_{\mathcal{P}8} = 36$ for Ori-AFDM-$(6, 8)$, respectively. With $d_0 = 2$, the corresponding normalized MEDs of these two schemes are

$$d_1 = d_0/\sqrt{E_1} = 2/\sqrt{21} \approx 0.44, \tag{27}$$

and

$$d_2 = d_0/\sqrt{E_2} = 2/\sqrt{36} \approx 0.33, \tag{28}$$

respectively.

2) MC-AFDM-T2:

For the MC-AFDM-T2-$(4, 4)$, its multi-constellation is illustrated in Fig. 2, where the $\mathcal{P}4$ and $\mathcal{S}4$ are the same as those of the MC-AFDM-T1-$(4, 8)$, and the $\mathcal{L}4$ and $\mathcal{T}4$ are obtained by the additional optimal interpolation in the $\mathcal{P}8$ exploited in MC-AFDM-T1-$(4, 8)$. All legitimate vector patterns of MC-AFDM-T2-$(4, 4)$ can be represented by a set $\mathcal{M}_4 = \mathcal{S}_4 \cup \mathcal{T}_4$. Here $\mathcal{S}_4 = \{\mathbf{x}_1^{\mathcal{S}}, \mathbf{x}_2^{\mathcal{S}}, ..., \mathbf{x}_8^{\mathcal{S}}\}$, $\mathcal{T}_4 = \{\mathbf{x}_1^{\mathcal{T}}, \mathbf{x}_2^{\mathcal{T}}, ..., \mathbf{x}_8^{\mathcal{T}}\}$ and specific patterns in the set $\mathcal{M}_4$ are given by

$$\begin{aligned} \mathbf{x}_1^{\mathcal{S}} &= [P_4, P_4, P_4, P_4]^T, \ \mathbf{x}_2^{\mathcal{S}} = [P_4, P_4, S_4, S_4]^T, \\ \mathbf{x}_3^{\mathcal{S}} &= [P_4, S_4, P_4, S_4]^T, \ \mathbf{x}_4^{\mathcal{S}} = [P_4, S_4, S_4, P_4]^T, \\ \mathbf{x}_5^{\mathcal{S}} &= [S_4, P_4, P_4, S_4]^T, \ \mathbf{x}_6^{\mathcal{S}} = [S_4, P_4, S_4, P_4]^T, \\ \mathbf{x}_7^{\mathcal{S}} &= [S_4, S_4, P_4, P_4]^T, \ \mathbf{x}_8^{\mathcal{S}} = [S_4, S_4, S_4, S_4]^T, \end{aligned} \tag{29}$$

[2]**Theorem I** in [4], Under a doubly selective channel with a maximum delay $l_{\max}$ and maximum normalized Doppler shift $\alpha_{\max}$, AFDM achieves full diversity order if $2\alpha_{\max} + l_{\max} + 2\alpha_{\max} l_{\max} < N$.

TABLE I
THE MAIN SIMULATION PARAMETERS

Number of subcarriers	$N = 4$, 6
Length of chirp-periodic prefix	$L = 2$
Carrier frequency	$f_c = 4$ GHz
Chirp subcarrier spacing	$\Delta f = 2$ kHz
Bandwidth	$B = 8$ kHz, 12 kHz
Number of multi-path components	$P = 2$, 3
Maximum delay spread	$l_{\max} = 1$
Maximum normalized Doppler shift	$\epsilon_{\max} = 1$
Maximum speed	$v_{\max} = 540$ km/h
Channel gain	$h \sim \mathcal{CN}(0, \frac{1}{P})$
AFDM parameters	$c_1 = \frac{2\alpha_{\max}+1}{2N}$, $c_2 = \frac{1}{2\pi}$

TABLE II
DELAY-DOPPLER PROFILE FOR DIFFERENT CHANNELS

Parameter	2-path channel	3-path channel
Delay spread l	$(0, 1)$	$(0, 0, 1)$
Normalized Doppler shift ϵ	$(0, 1)$	$(0, 1, 1)$

and

$$\begin{aligned}
&\mathbf{x}_1^{\mathcal{T}} = [L_4, L_4, L_4, L_4]^T,\ \mathbf{x}_2^{\mathcal{T}} = [L_4, L_4, T_4, T_4]^T,\\
&\mathbf{x}_3^{\mathcal{T}} = [L_4, T_4, L_4, T_4]^T,\ \mathbf{x}_4^{\mathcal{T}} = [L_4, T_4, T_4, L_4]^T,\\
&\mathbf{x}_5^{\mathcal{T}} = [T_4, L_4, L_4, T_4]^T,\ \mathbf{x}_6^{\mathcal{T}} = [T_4, L_4, T_4, L_4]^T,\\
&\mathbf{x}_7^{\mathcal{T}} = [T_4, T_4, L_4, L_4]^T,\ \mathbf{x}_8^{\mathcal{T}} = [T_4, T_4, T_4, T_4]^T.
\end{aligned} \tag{30}$$

For the above two groups of vector patterns, the MC-AFDM-T2 can be regarded as the combination of two specific cases of MC-AFDM-T1, i.e., MC-AFDM-T1 with $(\mathcal{P}_4, \mathcal{S}_4)$ and $(\mathcal{L}_4, \mathcal{T}_4)$. All legitimate patterns utilizing the same modulation order of 4, and the SE is $\eta_{\text{T2-(4, 4)}} = \frac{\log_2|\mathcal{M}_4|+4\log_2 M}{N} = \frac{\log_2 16+4\log_2 4}{4} = 3$ bits/s/Hz. As depicted in Fig. 2, the average symbol energy of $\mathcal{P}4$, $\mathcal{S}4$, $\mathcal{L}4$ and $\mathcal{T}4$ can be calculated as $E_{\mathcal{P}4} = 4$, $E_{\mathcal{S}4} = 2$, $E_{\mathcal{L}4} = 3$ and $E_{\mathcal{T}4} = 3$, respectively. Thus, the average energy of the patterns in $\mathcal{M}_4$ is

$$\begin{aligned}
E_{\text{ave}}^{\mathcal{M}_4} &= \frac{1}{|\mathcal{M}_4|}(E_{\mathbf{x}_1^{\mathcal{S}}} + E_{\mathbf{x}_2^{\mathcal{S}}} + ... + E_{\mathbf{x}_8^{\mathcal{S}}})\\
&\quad + \frac{1}{|\mathcal{M}_4|}(E_{\mathbf{x}_1^{\mathcal{T}}} + E_{\mathbf{x}_2^{\mathcal{T}}} + ... + E_{\mathbf{x}_8^{\mathcal{T}}})\\
&= \frac{4E_{\mathcal{P}4}}{16} + \frac{4E_{\mathcal{S}4}}{16} \cdots\cdots (\text{for } \mathbf{x}_1^{\mathcal{S}}, \mathbf{x}_8^{\mathcal{S}})\\
&\quad + \frac{6(2E_{\mathcal{P}4} + 2E_{\mathcal{S}4})}{16} \cdots\cdots (\text{for } \mathbf{x}_2^{\mathcal{S}} \sim \mathbf{x}_7^{\mathcal{S}})\\
&\quad + \frac{4E_{\mathcal{L}4}}{16} + \frac{4E_{\mathcal{T}4}}{16} \cdots\cdots (\text{for } \mathbf{x}_1^{\mathcal{T}}, \mathbf{x}_8^{\mathcal{T}})\\
&\quad + \frac{6(2E_{\mathcal{L}4} + 2E_{\mathcal{T}4})}{16} \cdots\cdots (\text{for } \mathbf{x}_2^{\mathcal{T}} \sim \mathbf{x}_7^{\mathcal{T}})\\
&= 12.
\end{aligned} \tag{31}$$

Then, we have $E_1 = E_{\text{ave}}^{\mathcal{M}_4} = 12$ for MC-AFDM-T2-$(4, 4)$. With $d_0 = 2$, the corresponding normalized MEDs of MC-AFDM-T2-$(4, 4)$ and Ori-AFDM-$(4, 8)$ are

$$d_1 = d_0/\sqrt{E_1} = 2/\sqrt{12} \approx 0.58, \tag{32}$$

and

$$d_2 = d_0/\sqrt{E_2} = 2/\sqrt{24} \approx 0.41, \tag{33}$$

respectively.

In addition, the case of MC-AFDM-T2-$(6, 4)$ is similar to case of extending MC-AFDM-T1-$(4, 8)$ to MC-AFDM-T1-$(6, 8)$. Due to the limited length of this paper, the details for MC-AFDM-T2-$(6, 4)$ are omitted.

III. ANALYSIS OF MEDS

With the de-normalized signal contestations depicted in Figs. 1 and 2, we have

$$d_{(\text{MC-AFDM-T1/T2})} = d_{(\text{Ori-AFDM})} = d_0, \tag{34}$$

and with E_1 for MC-AFDM-T1/T2, and E_2 for Ori-AFDM, the normalized MEDs are

$$d_1 = d_0/\sqrt{E_1},\ d_2 = d_0/\sqrt{E_2}. \tag{35}$$

Since $E_1 < E_2$, $d_1 > d_2$, SNR gains can be achieved.

Comparisons of normalized MEDs of MC-AFDM-T1/T2 and Ori-AFDM with more values of (N, M) are given here.

A. MEDs of MC-AFDM-T1

- $N = 4$, $M = 16$, $d_0 = 2, E_1 = 28, E_2 = 40 \rightarrow$
  $d_1 = d_0/\sqrt{E_1} \approx 0.37, d_2 = d_0/\sqrt{E_2} \approx 0.32$;
- $N = 6$, $M = 16$, $d_0 = 2$, $E_1 = 42$, $E_2 = 60 \rightarrow$
  $d_1 = d_0/\sqrt{E_1} \approx 0.31, d_2 = d_0/\sqrt{E_2} \approx 0.26$;
- $N = 8$, $M = 16$, $d_0 = 2$, $E_1 = 52$, $E_2 = 80 \rightarrow$
  $d_1 = d_0/\sqrt{E_1} \approx 0.28, d_2 = d_0/\sqrt{E_2} \approx 0.22$;

B. MEDs of MC-AFDM-T2

- $N = 4$, $M = 8$, $d_0 = 2$, $E_1 = 22$, $E_2 = 40 \rightarrow$
  $d_1 = d_0/\sqrt{E_1} \approx 0.43, d_2 = d_0/\sqrt{E_2} \approx 0.32$;
- $N = 6$, $M = 8$, $d_0 = 2$, $E_1 \approx 33$, $E_2 = 60 \rightarrow$
  $d_1 = d_0/\sqrt{E_1} \approx 0.35, d_2 = d_0/\sqrt{E_2} \approx 0.26$;
- $N = 8$, $M = 8$, $d_0 = 2$, $E_1 = 48$, $E_2 = 80 \rightarrow$
  $d_1 = d_0/\sqrt{E_1} \approx 0.29, d_2 = d_0/\sqrt{E_2} \approx 0.22$;

It can be observed from the above comparisons, the proposed MC-AFDM-T1 and MC-AFDM-T2 schemes achieve larger normalized MEDs than these of Ori-AFDM.

IV. SIMULATIONS AND DISCUSSIONS

Assuming that the channel state information (CSI) is known at the receiver, Monte Carlo simulations are carried out under doubly-selective channels with the delay-profile of $(l_{\max}, \epsilon_{\max}, P) = (1, 1, 2)$ and $(1, 1, 3)$. Details of the main simulation parameters are summarized in Tables I and II. ML detection is employed to recover AFDM vectors for further SER calculations.

Figs. 3 and 4 present the SER performance of the three AFDM-based schemes at the SE of 3 bits/s/Hz for $N = 4$ and 6, respectively. It can be observed that by exploiting the hybrid

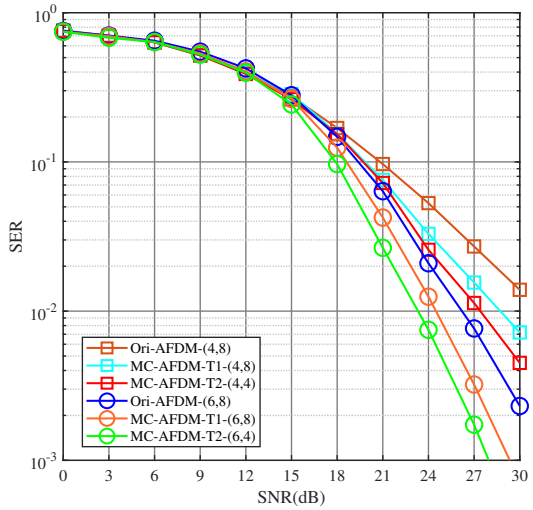

Fig. 3. SERs of MC-AFDM-T1, MC-AFDM-T2 and Ori-AFDM under integer Doppler shifts, $P = 2$, $\eta = 3$ bits/s/Hz.

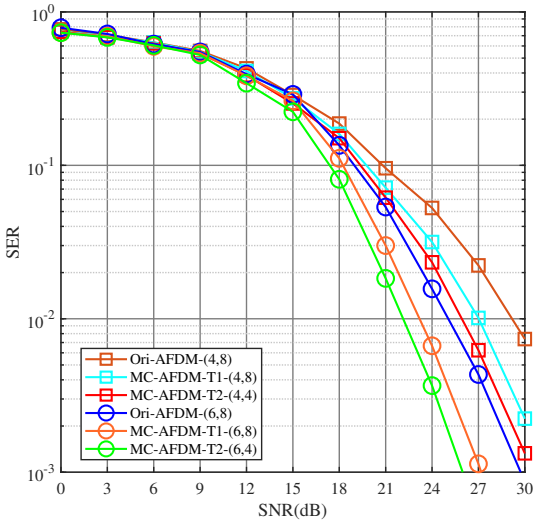

Fig. 4. SERs of MC-AFDM-T1, MC-AFDM-T2 and Ori-AFDM under integer Doppler shifts, $P = 3$, $\eta = 3$ bits/s/Hz.

of high-order and low-order modulations, the proposed MC-AFDM-T1 and MC-AFDM-T2 schemes consistently achieve better error performance than the Ori-AFDM, while maintaining the same SE. Specifically, under the doubly-selective channels with two multi-path components ($P = 2$), MC-AFDM-T1 achieves SNR gains of about 2 dB for the case of $N = 4$ and 1.5 dB for $N = 6$ at the SER of 10^{-2}, respectively. Additionally, MC-AFDM-T1 achieves SNR gains of about 3 dB for both $N = 4$ and $N = 6$. For the results in Fig. 4, the MC-AFDM-T2 schemes achieve approximate gains of 3 dB at SER of 10^{-2} for $N = 4$ and of 4 dB at the SER of 10^{-3} for $N = 6$, respectively.

V. CONCLUSIONS

In this paper, we have studied signal designs for AFDM by exploiting the hybrid multi-constellations. Compared with conventional scheme, improved SER has been achieved. The core idea of obtaining the proposed hybrid multi-constellations is by eliminating outer points with the highest energy and using geometric interpolation on the single ordinary constellation. This leads to a high transmission rate and with a lower order modulations. Monte Carlo simulations have demonstrated the SER superiority of the proposed MC-AFDM-T1 and MC-AFDM-T2 over the original AFDM scheme and their potential for future 6G systems, especially for high-mobility scenarios.

REFERENCES

[1] IMT-2030 (6G) Promotion Group, "White paper on 6G vision and candidate technologies," 2021.

[2] A. Bemani, N. Ksairi, and M. Kountouris, "AFDM: A full diversity next generation waveform for high mobility communications," in *Proc. IEEE Int. Conf. on Commun. Workshops (ICC Workshops)*, Montreal, QC, Canada, Jun. 2021, pp. 1–6.

[3] A. Bemani, N. Ksairi, and M. Kountouris, "Low complexity equalization for afdm in doubly dispersive channels," in *Proc. IEEE Int. Conf. on Acoustics, Speech, and Signal Process. (ICASSP)*. Singapore, Singapore, May 2022, pp. 5273-5277.

[4] A. Bemani, N. Ksairi, and M. Kountouris, "Affine frequency division multiplexing for next generation wireless communications," *IEEE Trans. Wireless Commun.*, vol. 22, no. 11, pp. 8214-8229, Nov. 2023.

[5] H. Yin and Y. Tang, "Pilot aided channel estimation for AFDM in doubly dispersive channels," *IEEE/CIC Int. Conf. Commun. China (ICCC) 2022*, Sanshui, Foshan, China, 2022, pp. 308-313.

[6] Y. Ni, Z. Wang, P. Yuan, and Q. Huang, "An AFDM-based integrated sensing and communications," in *Proc. Int Symposium Wireless Commun. Syst. (ISWCS)*, Hangzhou, China, 2022, pp. 1-6.

[7] A. Bemani, N. Ksairi, and M. Kountouris, "Integrated sensing and communications with affine frequency division multiplexing," *IEEE Wireless Commun. Lett.*, vol. 13, no. 5, pp. 1255-1259, May 2024.

[8] J. Zhu, *et al.*, "AFDM-based bistatic integrated sensing and communication in static scatterer environments," *IEEE Wireless Commun. Lett.*, vol. 13, no. 8, pp. 2245-2249, Aug. 2024.

[9] F. Liu, *et al.*, "Joint radar and communication design: Applications, state-of-the-art, and the road ahead," *IEEE Trans. Commun.*, vol. 68, no. 6, pp. 3834–3862, Jun. 2020.

[10] M. F. Keskin, H. Wymeersch, and V. Koivunen, "MIMO-OFDM joint radar-communications: Is ICI friend or foe?", *IEEE J. Sel. Topics Signal Process.*, vol. 15, no. 6, pp. 1393-1408, Nov. 2021.

[11] T. Mao, *et. al.,* "Novel index modulation techniques: A survey", *IEEE Commun. Surveys Tuts*., vol. 21, no. 1, pp. 315-348, 1st Quart. 2018.

[12] E. Basar, U. Aygölü, E. Panayırcı, and H. V. Poor, "Orthogonal frequency division multiplexing with index modulation," *IEEE Trans. Signal Process*., vol. 61, no. 22, pp. 5536–5549, Nov. 2013.

[13] Y. Shi, K. Gao, J. Zhu, X. Lu, and S. Wang, "Orthogonal frequency division multiplexing with joint subblocks index modulation," *IEEE Access*, vol. 7, pp. 23930–23939, Feb. 2019.

[14] M. Wen, E. Basar, Q. Li, B. Zheng, and M. Zhang, "Multiple-mode orthogonal frequency division multiplexing with index modulation," *IEEE Trans. Commun*., vol. 65, no. 9, pp. 3892–3906, Sep. 2017.

[15] M. Wen, Q. Li, E. Basar, and W. Zhang, "Generalized multiple-mode OFDM with index modulation," *IEEE Trans. Wireless Commun*., vol. 17, no. 10, pp. 6531–6543, Oct. 2018

[16] F. Yarkin and J. P. Coon, "Q-Ary multi-mode OFDM with index modulation," *IEEE Wireless Commun. Lett.*, vol. 9, no. 7, pp. 1110-1114, Jul. 2020.

[17] X. Ning, *et al.,* "OFDM with dual frequency index modulation," *IEEE Commun. Lett.*, vol. 26, no. 3, pp. 617-621, Mar. 2022.

[18] O. F. Tugtekin, A. T. Dogukan, E. Arslan, and E. Basar, "Coordinate interleaved OFDM with repeated In-phase/Quadrature index modulation," *IEEE Trans. Wireless Commun.*, vol. 23, no. 1, pp. 117-127, Jan. 2024.

[19] F. Yarkin and J. P. Coon, "Set partition modulation," *IEEE Trans. Wireless Commun.*, vol. 19, no. 11, pp. 7557-7570, Nov. 2020.

[20] F. Yarkin and J. P. Coon, "Index and composition modulation," *IEEE Commun. Lett.*, vol. 25, no. 3, pp. 911-915, Mar. 2021.

[21] T. Erseghe, N. Laurenti, and V. Cellini, "A multicarrier architecture based upon the affine Fourier transform," *IEEE Trans. Commun*., vol. 53, no. 5, pp. 853–862, May 2005.